A Novel Multistep Mechanism for Oxygen Binding to Ferrous Hemoproteins: Rapid Kinetic Analysis of Ferrous-Dioxy Myeloperoxidase (Compound III) Formation†

Husam M. Abu-Soud,*,‡ Frank M. Raushel,§ and Stanley L. Hazen||

Department of Obstetrics and Gynecology, The C.S. Mott Center for Human Growth and Development, 275 E. Hancock, Detroit, Michigan 48201, Department of Biochemistry and Molecular Biology, Wayne State University, Detroit, Michigan 48201, Department of Chemistry, Texas A&M University, College Station, Texas 77842, and Departments of Cell Biology and Cardiovascular Medicine and Center for Cardiovascular Diagnostics and Prevention, Cleveland Clinic Foundation, Cleveland, Ohio 44195

Received March 8, 2004; Revised Manuscript Received July 2, 2004

ABSTRACT: Myeloperoxidase (MPO), a hemoprotein that uses H_2O_2 as the electron acceptor in the catalysis of oxidative reactions, is implicated as a participant in inflammatory injury and cardiovascular diseases. Mechanisms for turning off this enzyme once released, preventing unwanted tissue injury, are poorly understood. We recently demonstrated that MPO heme reduction causes collapse of the heme pocket, as monitored by significant reductions in the rates of diatomic ligand binding to the heme iron. Using spectral and rapid kinetic measurements, we now demonstrate that molecular oxygen (O_2) binds to ferrous MPO (MPO−Fe(II)) in a distinct and novel mechanism. Rather than occurring through a simple, reversible, one-step mechanism, as is typical for O_2 binding to other ferrous hemoproteins, the reaction involves several kinetically and spectroscopically distinguishable intermediates. Diode array spectrophotometric and stopped-flow studies reveal that the formation of the MPO−Fe(II)−O_2 complex consists of at least three elementary steps and includes at least two sequential transient intermediates. The first step involves reversible formation of a transient intermediate via an O_2-dependent mechanism, followed by two sequential O_2-independent steps that appear to be conformational in origin. Insights into mechanisms for inactivating MPO and the novel mode of O_2 binding to the hemoprotein may provide important clues toward understanding the catalytic action of MPO.

Myeloperoxidase (MPO),[1] an abundant hemoprotein present in neutrophils and monocytes, plays an essential role in immune surveillance and innate host defense mechanisms (*1*). However, recent evidence also suggests that MPO contributes to oxidative tissue injury during inflammatory diseases and perhaps participates in the pathogenesis of cardiovascular disorders (*2*−*5*). Levels of MPO per leukocyte in patients strongly predict a risk for angiographic evidence of coronary artery disease (*6*), and plasma and serum levels of MPO predict a future risk of adverse cardiac outcomes in patients presenting chest pain (*7*) and acute coronary syndromes (*7*, *8*). Moreover, several genetic studies have recently demonstrated cardioprotective effects associated with subjects harboring functional polymorphisms in the MPO gene that lead to decreased MPO expression, as well as in subjects with MPO deficiency (*9*−*11*). Despite the many links between MPO and cardiovascular and inflammatory diseases, little is known about the factors that regulate its catalytic mechanism and structure. Indeed, current kinetic models suggest that catalytic activity of MPO is for the most part regulated by the availability of competing cosubstrates (*5*, *12*−*16*) and levels of nitric oxide (•NO, nitrogen monoxide), which at low levels is catalytically consumed by the enzyme but at elevated levels can form inactive nitrosyl complexes with the hemoprotein (*17*−*20*). Recently, we have demonstrated that MPO up-regulates the catalytic activity of inducible •NO synthase by preventing the catalytic activity inhibition that is attributed to nitrosyl complex formation (*21*).

In the ground state, MPO exists in the ferric (MPO−Fe(III)) form. MPO−Fe(III) reacts in a rapid and reversible manner with hydrogen peroxide (H_2O_2) to form compound I, a two-electron-oxidized intermediate possessing a ferryl oxy group and a resonance-stabilized porphyrin π cation radical (Fe(IV)═$O^{\bullet+\pi}$). This redox intermediate oxidizes halides and pseudohalides through a two-electron transition generating ground state (Fe(III)) MPO and the corresponding hypohalous acid. Hypohalous acids such as HOCl, the predominant oxidant formed by MPO under physiological

† This work was supported by National Institutes of Health Grants HL066367 and P01HL076491 and GRCR Grant Number 1M01RR018390.

* To whom correspondence should be addressed. Mailing address: Department of Obstetrics and Gynecology, Wayne State University, The C.S. Mott Center for Human Growth and Development, 275 E. Hancock, Detroit, MI 48201. Tel: 313/577-6178. Fax: 313/577-8554. E-mail: habusoud@med.wayne.edu.

‡ Wayne State University.

§ Texas A&M University.

|| Cleveland Clinic Foundation.

[1] Abbreviations: Fe(III), ferric; Fe(II), ferrous; H_2O_2, hydrogen peroxide; k_{on}, association rate constant; k_{off}, dissociation rate constant; EPO, eosinophil peroxidase; MPO, myeloperoxidase; NOS, nitric oxide synthase; NO, nitric oxide (nitrogen monoxide); CO, carbon monoxide.

10.1021/bi049541h CCC: $27.50
Published on Web 08/20/2004

levels of halides (*22*, *23*), play an important role in killing microorganisms (*24*, *25*). However, overproduction of halogenating oxidants can injure normal tissues by oxidative modification of proteins and lipoproteins, bleaching of heme groups, and oxidative destruction of electron transport chains (*26*, *27*). Like other peroxidases, MPO compound I can also oxidize multiple organic and inorganic compounds by two successive one-electron transitions generating radical species and the peroxidase intermediates compound II (Fe(IV)═O) and ground state Fe(III) enzyme (*5*, *12*−*16*). Oxidation of •NO by MPO occurs via this sequential pathway (*5*, *17*−*20*) and has been linked to endothelial dysfunction in cardiovascular disease and sepsis through catalytic consumption of •NO (*17*−*20*, *28*). Similarly, MPO may also use nitrite (NO_2^-), a major end product of •NO metabolism, as a one-electron substrate to generate nitrogen dioxide ($^{\bullet}NO_2$) (*29*), a diffusible radical implicated in both nitration of protein tyrosyl residues in vivo (*28*), and LDL modification and conversion into an atherogenic form (*27*−*32*).

Mechanisms for "shutting off" MPO activity are thus of considerable interest. MPO is highly resistant to protease and chemical inactivation, a property likely the result of evolutionary pressures for development of an enzyme that produces caustic reactive oxidant species within the harsh environs of the phagolysosomal compartment. Over 2 decades ago, it was recognized that heme reduction of MPO−Fe(III) converts the enzyme into an inactive ferrous MPO (MPO−Fe(II)) form (*12*). A variety of physiological reductants, including NADPH, ascorbate, and superoxide ($O_2^{\bullet-}$), can inhibit MPO catalysis (*12*). It has also been suggested that O_2 binding to MPO−Fe(II), and $O_2^{\bullet-}$ binding to MPO−Fe(III), each leads to formation of another inactive form, a ferrous dioxy intermediate termed compound III (MPO−Fe(II)−O_2) (*12*, *33*).

With the use of a combination of rapid kinetic methods and diatomic ligand binding studies with NO and CO, changes in the heme pocket environment attendant with heme reduction were monitored (*20*). A model was developed suggesting that MPO heme reduction is accompanied by significant alterations (collapse) in the heme environment, preventing access of substrates to the catalytic site of the enzyme (*20*). We now show that O_2 binding to MPO−Fe(II) proceeds through a complex multistep process, including generation of at least two kinetically and spectroscopically distinct transient Fe(II)−O_2-like intermediates. As far as we are aware, this behavior is unique among hemoprotein model compounds and advances our understanding of the catalytic cycle of MPO. Collectively, these kinetic behaviors distinguish MPO from other hemoprotein model compounds and provide a foundation to advance our understanding of the catalytic cycle of MPO.

EXPERIMENTAL PROCEDURES (MATERIALS AND METHODS)

Materials. O_2 gas was purchased from Matheson Gas products, Inc., and used without further purification. All other reagents and materials were of the highest purity grades available and obtained from either Sigma Chemical Co. or Aldrich.

Enzyme Purification. MPO was purified from detergent extracts of human leukocytes as described (*34*). Trace levels of contaminating eosinophil peroxidase were then removed by passage over a sulfopropyl Sephadex column (*35*). Purity of isolated MPO was established by demonstrating a Reinheitzal (RZ) value of >0.85 (A_{430}/A_{280}), by SDS PAGE analysis with Coomassie Blue staining, and by in-gel tetramethylbenzidine peroxidase staining to confirm no observable contaminating eosinophil peroxidase activity. Enzyme concentration was determined spectrophotometrically utilizing a molar extinction coefficient of 89 000 M^{-1} cm^{-1}/heme of MPO (*36*).

Optical Spectroscopy and Rapid Kinetic Measurements. Optical spectra were recorded on a Cary 100 UV−visible spectrophotometer at 25 °C. Anaerobic spectra were recorded using septum-sealed quartz cuvettes that were attached through quick-fit joints to an all-glass vacuum train system. MPO samples were made anaerobic by several cycles of evacuation and equilibrated with catalyst-deoxygenated N_2. Separate buffer solutions were evacuated, gassed with N_2, and anaerobically transferred either to the stopped-flow instrument or to anaerobic cuvettes using gastight syringes. Cuvettes were maintained under N_2 positive pressure during spectral measurements.

All kinetic measurements were performed with a temperature-controlled stopped-flow apparatus (180-π*, Applied Photophysics) equipped for anaerobic work. Measurements were carried out at 10 °C and initiated by rapidly mixing equal volumes of the enzyme solutions (0.86 μM) with buffer solution supplemented with increasing concentrations of O_2. The reaction for O_2 binding to MPO was monitored at wavelengths determined on the basis of the spectral changes that occur upon O_2 binding to MPO−Fe(II), as indicated in the text. In all cases, the MPO−Fe(III) samples were reduced by a slight molar excess of dithionite prior to mixing with O_2. In a control experiment, the reduced MPO sample was applied to a PD-10 Sephadex G-25-M column (Amersham Biosciences) equilibrated with an anaerobic phosphate buffer to eliminate any dithionite residual presence that may interfere in the reaction. The column was eluted with the same buffer under anaerobic conditions, and the enzyme sample was collected, adjusted to the desired concentration, and then transferred using Hamilton gastight syringe to the stopped-flow reservoir, which is maintained under nitrogen atmosphere. The MPO−Fe(II) and O_2 solutions were allowed to cool to 10 °C in syringes housed in the stopped-flow instrument (closed to the atmosphere) prior to mixing. In both cases, comparable results were observed monitoring the reaction of MPO−Fe(II) with O_2 indicating that residual dithionite present in the reaction system has no influence on the kinetic results. To determine the apparent rate constants for generation of MPO−Fe(II)−O_2 complex, the time course of absorbance change was fit to single ($Y = 1 - e^{-kt}$) or double ($Y = A\ e^{-kt} + B\ e^{-k2t} + C$) exponential functions using a nonlinear least-squares method provided by the instrument manufacturer. Signal-to-noise ratios were improved by averaging 7−10 individual traces for each experiment.

Solution Preparation. Anaerobic 0.2 M sodium phosphate buffer solutions, pH 7.0, containing various concentrations of O_2 were prepared by mixing different volumes of buffer saturated with O_2 gas at 21 °C with anaerobic buffer solution. Saturation was achieved by bubbling O_2 for 1 h in a septum-sealed flask at 21 °C. Final O_2 concentrations were calculated

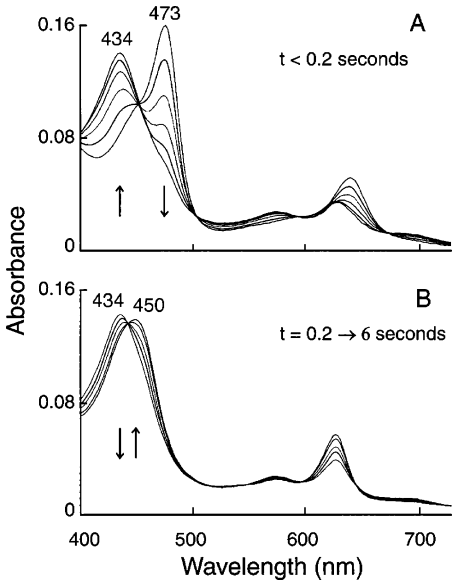

FIGURE 1: Formation of MPO−Fe(II)−O_2 complex. Diode array rapid scanning spectra for the intermediates and final product formed by reacting MPO−Fe(II) with air-saturating buffer at two sequential time frames are shown. Spectra traces were collected at 0.01, 0.05, 0.075, 0.1, 0.125, and 0.15 s (panel A) and at 0.2, 0.25, 0.3, 0.4, and 0.5 s (panel B) after mixing an anaerobic solution containing 3.6 μM MPO−Fe(II) with an equal volume of air-saturated buffer solution. Experiments were performed under anaerobic conditions in sodium phosphate buffer (200 mM, pH 7.0) at 10 °C. Arrows indicate the direction of spectral change over time as each intermediate advanced to the next.

on the basis of a saturating concentration of O_2 of ~1.2 mM at 21 °C and 1 atm pressure.

RESULTS

Initial Rapid Spectroscopic Characterization of O_2 Binding to Ferrous MPO. Addition of a slight molar excess of dithionite to MPO−Fe(III) caused immediate MPO heme iron reduction, as judged by a shift in the Soret absorbance peak from 430 to 473 nm, and the appearance of additional absorbance peaks in the visible range at 642 nm, as previously reported (*12*, *16*, *18*). To investigate more closely the formation of the MPO−Fe(II)−O_2 complex, compound III, we first monitored absorbance changes versus time upon mixing prereduced MPO (i.e., MPO−Fe(II)) with O_2-equilibrated buffer at 10 °C, using a diode array stopped-flow instrument. The characteristics of the spectral change occurring in the various time ranges through the reaction of MPO−Fe(II) with O_2 are shown in Figure 1, panels A and B. The variety of shapes of the reaction curves as a function of time indicates that the reaction involves several intermediates having different distinct spectral properties. The first set of the spectral alterations, of which the Soret spectrum was characterized by absorbance peak at 434 and additional visible peaks at 575, 627, and 700 nm (Figure 1, panel A), occurs within 0.2 s after mixing at 10 °C. These spectral changes were unstable and converted to the final form shown (Figure 1, panel B) within 6 s, as evidenced by a time-dependent shift in Soret and visible absorbance peaks to 450, 577, and 627 nm through isosbestic points located at 440, 547, 597, and 640 nm. The spectral changes that occur through the reaction of MPO−Fe(II) and O_2 differ from that observed with either ferric or ferrous forms of MPO, the

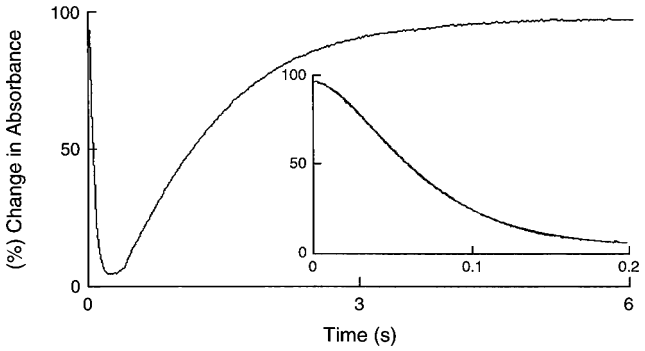

FIGURE 2: Single-wavelength stopped-flow traces for the reaction of MPO−Fe(II) with air-saturated buffer monitored at 460 nm. An anaerobic solution containing 1.0 μM MPO−Fe(II) [prepared by mixing MPO−Fe(III) with a slight molar excess of dithionite] was rapidly mixed with an equal volume of sodium phosphate buffer (200 mM, pH 7.0) supplemented with differing concentrations of O_2 at 10 °C. Experiments were carried out by monitoring the change in absorbance at 460 nm (where all the intermediates have been observed). The inset depicts the absorbance changes that occurred within the first 200 ms of the reaction.

Soret absorbance maxima of which are centered at 430 and 473 nm, respectively (*12*, *16*, *18*). However, the final spectral changes (Figure 1, panel B) are identical to that previously reported for MPO−Fe(II)−O_2 complex generated from either MPO−Fe(III) in the presence of NADH, O_2, and 2,4-dichlorophenol, which is known to be an activator of the aerobic oxidation of NADH by peroxidase, or from a direct reaction of MPO−Fe(II) and O_2 (*37*, *38*). Collectively, these results indicate that O_2 binds MPO−Fe(II) generating one or more transient intermediates before generating a more stable, low-spin, six-coordinate Fe(II)−O_2 complex, classically known as compound III.

Kinetic Analysis of O_2 Binding to Ferrous MPO. The time course for the appearance of MPO−Fe(II)−O_2 obtained at various single wavelengths indicates that the reaction is triphasic with sequential steps occurring at sufficiently different rates to enable each process to be studied by conventional stopped-flow methods. Experiments were performed under pseudo-first-order conditions by rapid mixing of equal volumes of MPO−Fe(II) with buffer solutions supplemented with different O_2 concentrations. A trace obtained at 460 nm, a wavelength selected because it permits kinetic assessment of both early and late phases of the reaction, is shown in Figure 2. An initial rapid absorbance decrease was observed, followed by a slower increase in absorbance. The inset to Figure 2 shows the change in absorbance at 460 nm that takes place during the first 0.20 s of the reaction. An initial lag phase in the curve (over the first 25 ms) was observed, indicating that a faster process not visible at this wavelength is involved. Consistent with this notion, the absorbance changes at 460 nm during the first 0.2 s of the reaction were best fitted to a double-exponential function with observed rate constants of 65 and 23 s^{-1}. The absorbance decrease at 460 nm was followed by a slower increase in absorbance, which was best fit to a single-exponential function with an observed pseudo-first-order rate constant of 0.73 s^{-1}. These results collectively support the presence of at least three sequential kinetically distinct intermediate reactions during the overall interaction between MPO−Fe(II) and O_2. In addition, comparable results were observed monitoring MPO−Fe(II) reaction with O_2

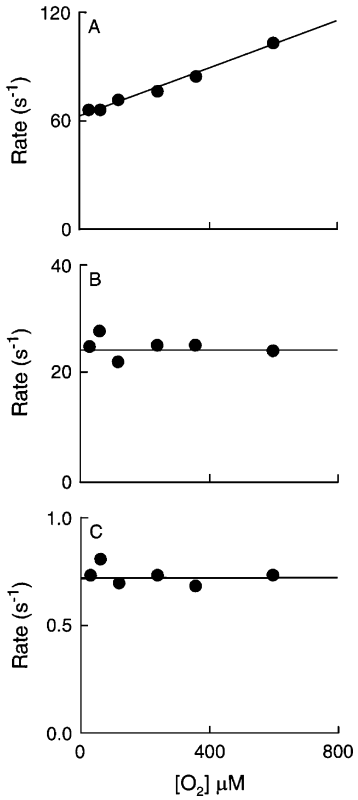

FIGURE 3: Effect of O_2 concentration on the formation of various oxygenated MPO−Fe(II) intermediates. Spectral changes and kinetic measurements indicate that the reactions are triphasic. Panel A plots the observed rates for the formation of the first phase ([MPO−Fe(II)−O_2]′) versus O_2 concentration, while panel B plots the observed rates for the formation of the second and third phases ([MPO−Fe(II)−O_2]″ and MPO−Fe(II)−O_2, respectively) versus O_2 concentration.

following removal of any residual dithionite by passage of the prereduced MPO sample over a desalting column. This behavior indicates that residual dithionite present in the reaction solution has no impact on the kinetic results.

Because of the unusual nature of MPO−Fe(II)−O_2 interactions, we further examined the kinetics of formation of the transient intermediate species as a function of O_2 concentration. Pseudo-first-order rate constants of their formation were ascertained and plotted as a function of O_2 concentration (Figure 3). The plot of the pseudo-first-order rate constant for the initial Fe(II)−O_2 complex (kinetically modeled and detected as the lag phase in the initial reaction; Figure 2 insert) was linear with a positive intercept, indicating that formation of the first detectable intermediate is O_2-dependent and reversible and proceeds through a simple, one-step mechanism with k_{on} of 7.1×10^4 M^{-1} s^{-1} and k_{off} of 63 s^{-1} (Figure 3, panel A). The subsequent conversion of this intermediate into the kinetically and spectroscopically distinct second and third intermediates occurred via mechanisms independent of O_2 concentration (Figure 3, panels B and C), indicating that these steps are both irreversible and likely conformational in nature.

DISCUSSION

For over 100 years, biochemists have studied the binding of molecular O_2 to hemoproteins such as hemoglobin, both because of its importance to various biological functions and because of the ease with which it may be monitored. Upon

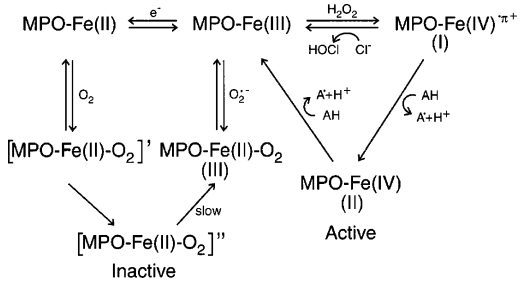

FIGURE 4: A kinetic model accounting for the complex mechanism of O_2 binding to MPO−Fe(II), incorporated within the context of the classic peroxidase cycle.

O_2 binding to the iron atom of hemoproteins, marked alterations in the spectral properties of the prosthetic group typically occur, a process known as a shift in the Soret absorbance spectrum (*39*−*51*). In all cases thus far described, O_2 binding occurs through a simple, either one- or two-step process (*39*−*51*). In a one-step model (e.g., E + O_2 ↔ EO_2), increasing O_2 concentration results in an ever-increasing observed pseudo-first-order rate constant of binding to the heme moiety (*52*). In a two-step mechanism (e.g., E + O_2 ↔ E′−O_2 ↔ E″−O_2), the rate of O_2 binding to the heme exhibits saturation at some finite value governed by the first-order process described by E + O_2 ↔ E′−O_2 (*52*). A multiple-step mechanism may also be detected by the observation of more than one transient phase upon mixing O_2 and hemoprotein. This could be provoked by either a significantly different rate constant for each phase or changes in extinction coefficient between E′−O_2 and E″−O_2 or both. Even for O_2 binding to the R vs T conformers of hemoglobin, the observed interaction between O_2 and the heme prosthetic group may be described by these simple reversible mechanisms (*51*). Therefore, one of the most remarkable findings of the present study is the unusual multistep mechanism governing O_2 binding to the heme of ferrous MPO.

A kinetic model accounting for the complex mechanism of O_2 binding to MPO−Fe(II), within the context of the classic peroxidase cycle, is shown in Figure 4. MPO exists as a variety of interchangeable catalytic intermediates that differ in oxidation state, form of oxygen binding, catalytic activity, and conformation. These intermediate forms generate at least two interconnecting cycles, one active and another inactive (Figure. 4). The "active cycle", also termed the "classic peroxidase cycle" of heme peroxidases, describes various intermediate forms of MPO (compounds I and II) capable of executing one- and two-electron oxidation reactions with numerous organic and inorganic compounds. The "inactive cycle" consists of the reduction of ground-state MPO into its ferrous form and the newly appreciated multistep pathway necessary for its reentrance into the catalytic cycle via interactions with O_2 and subsequent formation of compound III (Figure 4).

Rapid mixing of MPO−Fe(II) with O_2 ultimately generates a relatively stable ferrous dioxy complex (MPO−Fe(II)−O_2) with Soret absorbance and visible optima at 450 and 625 nm, previously termed "compound III" (*12*, *37*, *38*). The present studies, however, reveal that at least three distinct ferrous-dioxy intermediate forms of MPO exist, which may be kinetically described by the following equation (Figure 4):

$$\text{MPO}-\text{Fe(II)} + \text{O}_2 \underset{k_{-1}}{\overset{k_1}{\leftrightarrow}} [\text{MPO}-\text{Fe(II)}-\text{O}_2]' \xrightarrow{k_2} [\text{MPO}-\text{Fe(II)}-\text{O}_2]'' \xrightarrow{k_3} \text{MPO}-\text{Fe(II)}-\text{O}_2 \overset{k_4}{\leftrightarrow} \text{MPO}-\text{Fe(III)} + \text{O}_2^{\bullet-}$$

Figure 1 (panel A) represents spectral changes produced upon initial binding of O_2 to MPO−Fe(II). During the first 200 ms of the reaction, the rapid sequential formation of two transient intermediates occurs, [MPO−Fe(II)−O_2]′ and [MPO−Fe(II)−O_2]″, accompanied by an initial lag phase, and then an overall shift in Soret absorbance and visible optima from 473 and 638 to 435, 573, and 630 nm. A single set of isosbestic points were observed over this time frame, suggesting formation of one intermediate in the initial reaction. The spectral changes at 460 nm over this time interval reveals the presence of a lag phase with the kinetic tracing over the initial 200 ms of reaction best fit using two exponential functions (Figure 2 inset). These findings demonstrate that not one but at least two sequential kinetically distinct intermediates are formed during the initial binding of O_2 to MPO−Fe(II), the first ([MPO−Fe(II)−O_2]′, corresponding to the lag phase) possessing similar spectral characteristics to the native enzyme (MPO−Fe(II)). Kinetic analyses reveal that formation of [MPO−Fe(II)−O_2]′ and [MPO−Fe(II)−O_2]″ are clearly distinguishable by their differing response to varying O_2 concentrations (Figure 3, panels A and B). The initial reaction proceeds through an O_2-dependent process, as shown by the positive slope ($k_1 = 7.1 \times 10^4$ M^{-1} s^{-1}) obtained when O_2 concentration is plotted against observed pseudo-first-order rate constant for binding (Figure 3, panel A). The positive *Y* intercept, which corresponds to a first-order dissociation rate constant (k_{-1} of 63 s^{-1}), confirms the reversible nature of this reaction. This dissociation rate constant is also relatively fast compared to that reported for other model Fe(II)−O_2 interactions (*39*−*51*). In contrast, the conversion from [MPO−Fe(II)−O_2]′ to [MPO−Fe(II)−O_2]″ proceeds through an irreversible, O_2-independent process, as revealed when O_2 concentration is plotted against observed first-order rate constant ($k_2 = 23$ s^{-1}) (Figure 3, panel B). Finally, the penultimate "MPO−compound III"-like spectral intermediate is formed during the ensuing 6 s of the reaction with Soret absorbance and visible optima at 450 and 625 nm (Figure 1, panel B). This final reaction proceeds through a single irreversible, O_2 -independent reaction, as judged by one set of isosbestic points (Figure 1, panel B) and the lack of O_2-dependence on the observed first-order rate constant ($k_3 = 0.73$ s^{-1}; Figure 3, panel C).

A narrowing or collapse in the heme pocket geometry upon MPO heme reduction may result from a significant increase in the affinity of the heme iron toward a sixth ligand, provided by either a water molecule or one of the amino acids located above the heme prosthetic group (*20*, *53*−*55*). Indeed, kinetic characterization of the binding of CO and NO to MPO ferric and ferrous forms was recently used to demonstrate that reduction of the MPO heme moiety significantly restricts access of diatomic ligands to the heme catalytic site (*20*). The results of the present studies demonstrate that O_2 binding to MPO−Fe(II) is also significantly influenced by steric constraints in the distal heme pocket, as manifest through the observed unusual multistep kinetic mechanism (Figure 4). Taken together, kinetic interrogations of the heme environment of ferrous MPO through diatomic ligand binding studies strongly support the hypothesis that tertiary structural alterations of the MPO−Fe(II) heme pocket serve as the primary determinant governing the reaction mechanism of O_2, CO, and NO binding to the enzyme.

Classically, it is generally believed that the mammalian heme peroxidase superfamily contains at least two additional pathways for the formation of ferrous-dioxy complex—superoxide addition to ferric enzyme and H_2O_2 addition to compound II (*12*, *16*, *33*, *56*, *57*). Direct reaction between ground-state enzyme and $O_2^{\bullet-}$ to generate compound III is a common and biologically significant route, as evidenced in studies employing activated neutrophils (*12*, *16*, *33*). Previous in vitro studies by Kettle and co-workers have demonstrated that the formation of MPO−Fe(II)−O_2 complex through this route is fast, displays a second-order rate constant of 2×10^6 M^{-1} s^{-1}, and occurs via a simple one-step mechanism (*12*, *33*). This finding is consistent with the notion that at ground state, MPO−Fe(III) exhibits a relatively open heme pocket geometry that permits easy access of $O_2^{\bullet-}$ to the MPO heme iron (*20*). A second alternative pathway for compound III formation has been reported for multiple members of the mammalian heme peroxidase superfamily (MPO, lactoperoxidase (LPO), and eosinophil peroxidase (EPO))—reaction of a large excess of H_2O_2 with compound II. However, formation of compound III via this mechanism is unlikely to occur in vivo since the reaction is relatively slow and is not detectable at physiologically plausible levels of H_2O_2 (*12*, *16*, *56*, *57*).

The MPO−Fe(II)−O_2 complex is extremely stable under anaerobic conditions. Formation of this stable MPO intermediate is thought to inhibit overall catalytic activity of heme peroxidases. Previous spectroscopic studies demonstrated that decay of compound III to native enzyme apparently occurs without any detectable intermediate and with a $t_{1/2}$ of ∼15 min at 25 °C (*37*, *58*−*60*). Instability of MPO−Fe(II)−O_2 complex is significantly enhanced in basic solution, as well as in the presence of superoxide dismutase (*37*, *58*−*60*). Kinetic measurements carried out on MPO indicated that ascorbic acid reduces compound III to native enzyme with a second-order rate constant of $(4.0 \pm 0.1) \times 10^2$ M^{-1} s^{-1} (*61*). Reduction of compound III by ascorbic acid has potential physiological relevance since it could help regenerate active ferric MPO, which may then enter into the catalytic cycle. Compound III is also able to react with a second molecule of $O_2^{\bullet-}$ yielding compound I, which in the presence of Cl^- is converted into native (MPO−Fe(III)) enzyme and HOCl (*61*).

Furthermore, our preliminary studies examining oxygen binding to ferrous LPO and EPO indicated that the buildup of LPO−Fe(II)−O_2 and EPO−Fe(II)−O_2 complexes follow a simple reversible one-step mechanism with second-order rate constants of 3.8×10^4 and 3.7×10^4 M^{-1} s^{-1}, respectively (Abu-Soud, unpublished results). Decay of the EPO−Fe(II)− and LPO−Fe(II)−O_2 complexes were independent of O_2 concentration and occurred via a one- or two-step mechanism depending on the experimental condition. This kinetic behavior is again typical for other hemoproteins but not the complex triphasic behavior noted for MPO. Therefore, O_2 binding to MPO−Fe(II) is unique among other

members of the mammalian heme-peroxidase superfamily and from that described in the literature of other hemoproteins (i.e., none follow a multistep mechanism as is observed for MPO).

In summary, the interaction of ferrous MPO with molecular oxygen is distinct from that observed with other hemoproteins, illustrating a complex multistep process. The affinity of ferrous MPO with O_2 is lower than that observed with other ferrous hemoprotein model compounds and consistent with a model where conformational changes in the heme pocket environment dominate the interaction (*17*, *20*). The stopped-flow data present herein and that previously reported for NO and CO binding to both ferrous and ferric forms of MPO (*17*, *20*) provide a wealth of information that allow us to obtain new insights into the structure−function relationship of MPO catalysis.

REFERENCES

1. Klebanoff, S. J., and Clark, R. A. (1978) *The Neutrophil: Functions and Clinical Disorders*, pp 1−810, Elsevier Science Publisher B. V., Amsterdam.
2. Hazen, S. L., and Heinecke, J. W. (1997) 3-Chlorotyrosine, a specific marker of myeloperoxidase-catalyzed oxidation, is markedly elevated in low-density lipoprotein isolated from human atherosclerotic intima, *J. Clin. Invest. 99*, 2075−2081.
3. Heinecke, J. W. (1998) Oxidants and antioxidants in the pathogenesis of atherosclerosis: implications for the oxidized low-density lipoprotein hypothesis, *Atherosclerosis 141*, 1−15.
4. Davies, M. J., Fu, S., Wang, H., and Dean, R. T. (1999) Stable markers of oxidant damage to proteins and their application in the study of human disease, *Free Radical Biol. Med. 27*, 1151−1163.
5. Podrez, E. A., Abu-Soud, H. M., and Hazen, L. H. (2000) Myeloperoxidase-generated oxidants and atherosclerosis, *Free Radical Biol. Med. 28*, 1717−1725.
6. Brennan, M. L., and Hazen, S. L. (2003) Emerging role of myeloperoxidase and oxidant stress markers in cardiovascular risk assessment, *Curr. Opin. Lipidol. 14*, 353−359.
7. Brennan M. L., Penn M. S., van Lente F., Nambi V., Shishehbor M. H., Aviles R. J., Goormastic M., McErlean E. S., Topol E. J., Nissen S. E., and Hazen, S. L. (2003) Prognostic Value of Myeloperoxidase in Patients with Chest Pain, *N. Engl. J. Med. 349*, 1595−1604.
8. Baldus, S., Heeschen, C., Meinertz, T., Zeiher A. M., Eiserich J. P., Munzel, T., Simoons M. L, and Hamm, C. W. (2003) Myeloperoxidase serum levels predict risk in patients with acute coronary syndromes, *Circulation 108*, 1440−1445.
9. Pecoits-Filho, R., Stenvinkel, P., Marchlewska, A., Heimburger, O., Barany, P., Hoff, C. M., Holmes, C. J., Suliman, M., Lindholm, B., Schalling, M., and Nordfors, L. (2003) A functional variant of the myeloperoxidase gene is associated with cardiovascular disease in end-stage renal disease patients, *Kidney Int. Suppl. 84*, S172−S176.
10. Nikpoor, B., Turecki, G., Fournier, C., Theroux, P., and Rouleau, G. A. (2001) A functional myeloperoxidase polymorphic variant is associated with coronary artery disease in French-Canadians, *Am. Heart J. 142*, 336−369.
11. Kutter, D., Devaquet, P., Vanderstocken, G., Paulus, J. M., Marchal, V., and Gothot, A. (2000) Consequences of total and subtotal myeloperoxidase deficiency: risk or benefit? *Acta Haematol. 104*, 10−15.
12. Kettle, A. J., and Winterbourn, C. C. (1997) Myeloperoxidase: a key regulator of neutrophil oxidant production, *Redox Rep. 3*, 3−15.
13. Bolscher, B. G., Zoutberrg, G. R., Cuperus, R. A., and Wever, R. (1984) Vitamin C stimulates the chlorinating activity of human myeloperoxidase, *Biochim. Biophys. Acta 784*, 189−191.
14. Marquez, L. A., Dunford, H. B., and Van Wart, H. (1990) Kinetic studies on the reaction of compound II of myeloperoxidase with ascorbic acid. Role of ascorbic acid in myeloperoxidase function, *J. Biol. Chem. 265*, 5666−5670.
15. Furtmuller, P. G., Obinger, C., Hsuanyu, Y., and Dunford, H. B. (2000) Mechanism of reaction of myeloperoxidase with hydrogen peroxide and chloride ion, *Eur. J. Biochem. 267*, 5858−5864.
16. Dunford, H. B. (1999) *Heme Peroxidases*, pp 349−385, Wiley-VCH, New York.
17. Abu-Soud, H. M., and Hazen, S. L. (2000) Nitric oxide modulates the catalytic activity of myeloperoxidase, *J. Biol. Chem. 275*, 5425−4530.
18. Abu-Soud, H. M., and Hazen, S. L. (2000) Nitric oxide is a physiological substrate for mammalian peroxidases, *J. Biol. Chem. 275*, 37524−37532.
19. Abu-Soud, H. M., Khassawneh, M. Y., Sohn, J. T., Murray, P., Haxhiu, M. A., and Hazen, S. L. (2001) Peroxidases inhibit nitric oxide (NO) dependent bronchodilation: development of a model describing NO-peroxidase interactions, *Biochemistry 40*, 11866−11875.
20. Abu-Soud, H. M., and Hazen, S. L. (2001) Interrogation of heme pocket environment of mammalian peroxidases with diatomic ligands, *Biochemistry 40*, 10747−10755.
21. Galijasevic, S., Saed, G. M., Diamond, M. P., and Abu-Soud, H. M. (2003) Myeloperoxidase up-regulates the catalytic activity of inducible nitric oxide synthase by preventing nitric oxide feedback inhibition, *Proc. Natl. Acad. Sci. U.S.A. 100*, 14766−14771.
22. Weiss, S. J., Klein, R, Slivka, A., and Wei, M. (1982) Chlorination of taurine by human neutrophils. Evidence for hypochlorous acid generation, *J. Clin. Invest. 70*, 598−607.
23. Harrison, J. E., and Schultz, J. (1976) Studies on the chlorinating activity of myeloperoxidase, *J. Biol. Chem. 251*, 1371−1374.
24. Klebanoff, S. J., Waltersdorph, A. M., and Rosen, H. (1984) Antimicrobial activity of myeloperoxidase, *Methods Enzymol. 105*, 399−403.
25. Albrich, J. M., McCarthy, C. A., and Hurst, J. K. (1981) Biological reactivity of hypochlorous acid: implications for microbicidal mechanisms of leukocyte myeloperoxidase, *Proc. Natl. Acad. Sci. U.S.A. 78*, 210−214.
26. Rosen, H., and Klebanoff, S. J. (1982) Oxidation of *Escherichia coli* iron centers by the myeloperoxidase-mediated microbicidal system, *J. Biol. Chem. 257*, 13737−13735.
27. Podrez, E. A., Febbraio, M., Sheibani, N., Schmitt, D., Silverstein, R. L., Hajjar, D. P., Cohen, P. A., Frazier, W. A., Hoff, H. F., and Hazen, S. L. (2000) Macrophage scavenger receptor CD36 is the major receptor for LDL modified by monocyte-generated reactive nitrogen species, *J. Clin. Invest. 105*, 1095−1108.
28. Eiserich, J. P., Hristova, M., Cross, C. E., Jones, A. D., Freeman, B. A., Halliwell, B., and van der Vliet, A. (1998) Formation of nitric oxide-derived inflammatory oxidants by myeloperoxidase in neutrophils, *Nature 391*, 393−397.
29. Brennan, M. L., Wu, W., Fu, X., Shen, Z., Song, W., Frost, H., Vadseth, C., Narine, L., Lenkiewicz, E., Borchers, M. T., Lusis, A. J., Lee, J. J., Lee, N. A., Abu-Soud, H. M., Ischiropoulos, H., and Hazen, S. L. (2002) A tale of two controversies: defining both the role of peroxidases in nitrotyrosine formation in vivo using eosinophil peroxidase and myeloperoxidase-deficient mice, and the nature of peroxidase-generated reactive nitrogen species, *J. Biol Chem. 277*, 17415−17427.
30. Podrez, E. A., Schmitt, D., Hoff, H. F., and Hazen S. L. (1999) Myeloperoxidase-generated reactive nitrogen species convert LDL into an atherogenic form in vitro, *J. Clin. Invest. 103*, 1547−1560.
31. van der Vliet, A., Eiserich, J. P., Halliwell, B., and Cross, C. E. (1997) Formation of reactive nitrogen species during peroxidase-catalyzed oxidation of nitrite. A potential additional mechanism of nitric oxide-dependent toxicity, *J. Biol. Chem. 272*, 7617−7625.
32. Burner, U., Furtmuller, P. G., Kettle, A. J., Koppenol, W. H., and Obinger, C. (2000) Mechanism of reaction of myeloperoxidase with nitrite, *J. Biol Chem. 275*, 20597−20601.
33. Kettle, A. J., Sangster, D. F., Gebicki, J. M., and Winterbourn, C. C. (1988*)* A pulse radiolysis investigation of the reactions of myeloperoxidase with superoxide and hydrogen peroxide, *Biochim. Biophys. Acta 956*, 58−62.
34. Rakita, R. M., Michel, B. R., and Rosen, H. (1990) Differential inactivation of *Escherichia coli* membrane dehydrogenases by a myeloperoxidase-mediated antimicrobial system, *Biochemistry 29*, 1075−1080.
35. Wever, R., Plat, H., and Hamers, M. N. (1981) Human eosinophil peroxidase: a novel isolation procedure, spectral properties and chlorinating activity, *FEBS Lett. 123*, 327−331.

36. Agner, K. (1963) Studies on myeloperoxidase activity, *Acta Chem. Scand. 17*, S332−S338.
37. Winterbourn, C. C, Garcia, R. C., and Segal, A. W. (1985) Production of the superoxide adduct of myeloperoxidase (compound III) by stimulated human neutrophils and its reactivity with hydrogen peroxide and chloride, *Biochem J. 228*, 583−592.
38. Odajima, T., and Yamazaki, I. (1970) Myeloperoxidase of the leukocyte of normal blood. I. Reaction of myeloperoxidase with hydrogen peroxide, *Biochim. Biophys. Acta 206*, 71−77.
39. Oprian, D. D., Gorsky, L. D., and Coon, M. J. (1983) Properties of the oxygenated form of liver microsomal cytochrome P-450, *J. Biol. Chem. 258*, 8684−8691.
40. Guengerich, F. P., Ballou, D. P., and Coon, M. J. (1976) Spectral intermediates in the reaction of oxygen with purified liver microsomal cytochrome P-450, *Biochem. Biophys. Res. Commun. 70*, 951−956.
41. Tyson, C. A., Lipscomb, J. D., and Gunsalus, I. C. (1972) The role of putidaredoxin and P450 cam in methylene hydroxylation, *J. Biol. Chem. 247*, 5777−5784.
42. Ishimura, Y., Ullrich, V., and Peterson, J. A. (1971) Oxygenated cytochrome P-450 and its possible role in enzymic hydroxylation, *Biochem. Biophys. Res. Commun. 42*, 140−146.
43. Peterson, J. A., Ishimura, Y., and Griffin, B. W. (1972) *Pseudomonas putida* cytochrome P-450: characterization of an oxygenated form of the hemoprotein, *Arch. Biochem. Biophys. 149*, 197−208.
44. Larroque, C., and Van Lier, J. E. (1980) The subzero temperature stabilized oxyferro complex of purified cytochrome P450scc, *FEBS Lett. 115*, 175−177.
45. Eisenstein, L., Debey, P., and Douzou, P. (1977) P450cam: oxygenated complexes stabilized at low temperature, *Biochem. Biophys. Res. Commun. 77*, 1377−1283.
46. Bonfils, C., Debey, P., and Maurel, P. (1979) Highly purified microsomal P-450: the oxyferro intermediate stabilized at low temperature, *Biochem. Biophys. Res. Commun. 88*, 1301−1307.
47. Abu-Soud, H. M, Gachhui, R, Raushel, F. M., and Stuehr, D. J. (1997) The ferrous-dioxy complex of neuronal nitric oxide synthase. Divergent effects of L-arginine and tetrahydrobiopterin on its stability, *J. Biol. Chem. 272*, 17349−17353.
48. Abu-Soud, H. M., Ichimori, K., Nakazawa, H., and Stuehr, D. J. (2001) Regulation of inducible nitric oxide synthase by self-generated NO, *Biochemistry 40*, 6876−6881.
49. Abu-Soud, H. M., Ichimori, K., Presta, A., and Stuehr, D. J. (2000) Electron transfer, oxygen binding, and nitric oxide feedback inhibition in endothelial nitric-oxide synthase, *J. Biol. Chem. 275*, 17349−17357.
50. Cooper, C. E. (1999) Nitric oxide and iron proteins, *Biochim. Biophys. Acta 1411*, 290−309.
51. Cassoly, R., and Gibson, Q. H. (1975) Conformation, cooperativity and ligand binding in human hemoglobin, *J. Mol. Biol. 91*, 301−313.
52. Hiromi, K. (1979) *Kinetics of Fast Enzyme Reactions: Theory and Practice*, Halsted Press Book, Kodansha Ltd., Tokyo.
53. Zeng, J., and Fenna, R. E. (1992) X-ray crystal structure of canine myeloperoxidase at 3 Å resolution, *J. Mol. Biol. 226*, 185−207.
54. Davey, C. A., and Fenna, R. E. (1996) 2.3 Å resolution X-ray crystal structure of the bisubstrate analogue inhibitor salicylhydroxamic acid bound to human myeloperoxidase: a model for a prereaction complex with hydrogen peroxide, *Biochemistry 35*, 10967−10974.
55. De Gioia, L., Ghibaudi, E. M., Laurenti, E., Salmona, M., and Ferrari, R. P. (1996) A theoretical three-dimensional model for lactoperoxidase and eosinophil peroxidase, built on the scaffold of the myeloperoxidase X-ray structure, *J. Biol. Inorg. Chem. 1*, 476−485.
56. Kohler, H., Taurog, A., and Dunford, H. B. (1988) Spectral studies with lactoperoxidase and thyroid peroxidase: interconversions between native enzyme, compound II, and compound III, *Arch. Biochem. Biophys. 264*, 438−449.
57. Hoogland, H., van Kuilenburg, A., van Riel, C., Muijsers, A. O., and Wever R. (1987) Spectral properties of myeloperoxidase compounds II and III, *Biochim. Biophys. Acta 916*, 76−82.
58. Hoogland, H., Dekker, H. L., van Riel, C., van Kuilenburg, A., Muijsers, A. O., and Wever, R. (1988) A steady-state study on the formation of Compounds II and III of myeloperoxidase, *Biochim. Biophys. Acta 955*, 337−345.
59. Cuperus, R. A., Muijsers, A. O., and Wever R. (1986) The superoxide dismutase activity of myeloperoxidase; formation of compound III, *Biochim. Biophys. Acta 871*, 78−84.
60. Zuurbier, K. W., van den Berg, J. D., Van Gelder, B. F., and Muijsers, A. O. (1992*)* Human hemi-myeloperoxidase. Initial chlorinating activity at neutral pH, compound II and III formation, and stability towards hypochlorous acid and high temperature, *Eur. J. Biochem. 205*, 737−742.
61. Marquez, L. A., and Dunford, H. B. (1990) Reaction of compound III of myeloperoxidase with ascorbic acid, *J. Biol. Chem. 265*, 6074−6078.

BI049541H